Photochemistry and Photobiology, Vol. 62, No. 5, pp. 830–835, 1995
Printed in the United States.

0031-8655/95 $05.00+0.00

AUTOFLUORESCENCE SPECTROSCOPY OF OPTICALLY TRAPPED CELLS

KARSTEN KÖNIG[1,2], YAGANG LIU[1,3], GREG J. SONEK[1,3], MICHAEL W. BERNS[1] and BRUCE J. TROMBERG*[1,4]

[1]Beckman Laser Institute and Medical Clinic, University of California, Irvine, CA 92715, USA;
[2]Institute for Molecular Biotechnology, D-07708 Jena, Germany;
[3]Department of Electrical and Computer Engineering, University of California, Irvine, CA 92715, USA and
[4]Department of Physiology and Biophysics, University of California, Irvine, CA 92715, USA

(*Received* 31 *March* 1995; *accepted* 29 *July* 1995)

Abstract—Cellular autofluorescence spectra were monitored in a single-beam gradient force optical trap ("optical tweezers") in order to probe the physiological effects of near infrared and UVA (320–400 nm) microirradiation. Prior to trapping, Chinese hamster ovary cells exhibited weak UVA-excited autofluorescence with maxima at 455 nm characteristic of β-nicotinamide adenine dinucleotide (phosphate) emission. No strong effect of a 1064 nm NIR microbeam on fluorescence intensity and spectral characteristics was found during trapping, even for power densities up to 70 MW/cm^2 and radiant exposures of 100 GJ/cm^2. In contrast to the 1064 nm trap, a 760 nm trapping beam caused a two-fold autofluorescence increase within 5 min (about 20 GJ/cm^2). Exposure to 365 nm UVA (1 W/cm^2) during 1064 nm trapping significantly altered cellular autofluorescence, causing, within 10 min, a five-fold increase and a 6 nm red shift *versus* initial levels. We conclude that 1064 nm microbeams can be applied for an extended period without producing autofluorescence changes characteristic of alterations in the cellular redox state. However, 760 nm effects may occur *via* a two-photon absorption mechanism, which, in a manner similar to UVA exposure, alters the redox balance and places the cell in a state of oxidative stress.

INTRODUCTION

Optical trapping of micrometer-sized dielectric particles is based on the radiation pressure of highly focused laser beams.[1,2] Dielectric particles, such as biological cells, can be polarized and trapped by the intensity gradients of strong electromagnetic fields in or near the beam focus. These trapped particles can then be moved without any physical contact by beam displacement (optical tweezers). The trapping forces, F, are directly proportional to the laser power P and can be determined by F = QP/c, where c is the velocity of light in the medium and Q is an efficiency parameter that depends on optical properties of the trapped object and laser beam quality. Typical values for the trapping forces are on the order of picoNewtons.

Optical traps have been used in biology and medicine for cell and organelle manipulation, cell fusion, cell sorting, *in vitro* fertilization and for the measurement of intrinsic mechanical forces of motile cells and cell organelles.[3–7] In the case of optical trapping of vital single cells, the trapping beam should possess a wavelength in the far red/near infrared (NIR)† spectral region, the so-called "optical window" for chlorophyll-free biological tissue. The lack of efficient endogenous absorbers in this region reduces the potential for cellular heating and death and avoids formation of competitive radiometric forces.

Typical *in situ* laser-trapping powers for motile cells (*e.g.* sperm cells) are on the order of 100 mW. Assuming a Gaussian distribution of the laser beam (TEM_{oo} mode) and an objective of 100× magnification with a numerical aperture (NA) of 1.3 as the focusing element, the diffraction-limited spot size d (diameter) at a given wavelength, λ, can be approximated by d = λ/NA.[8] At the commonly used 1064 nm trapping wavelength, the spot size will be reduced to about 800 nm and the spot area to about 5×10^{-9} cm^2. A 100 mW diffraction-limited trapping beam generates a trapping intensity of 20 MW/cm^2 and cells trapped for 1 min receive a radiant exposure of more than 1 GJ/cm^2.

This enormous photon flux density may place cells in a state of stress by inducing mechanical, thermal or chemical changes that affect cellular metabolism. One method for obtaining information on light-induced disturbances to metabolic function is monitoring intracellular fluorescence of the reduced coenzymes β-nicotinamide adenine dinucleotide (NADH) and β-nicotinamide adenine dinucleotide phosphate (NADPH). Fluorescent coenzymes (NADH, NADPH and flavins) act as highly sensitive bioindicators of respiratory chain activity. This was first recognized by Chance and Thorell[9] who studied intracellular oxygen status by means of nondestructive NADH fluorometry. An increase in NADH fluorescence has been found during ischemia, hypoxia and anoxia in the brain.[10] Lohmann[11] used the 365 nm excited autofluorescence for tumor detection. Differences in fluorescence intensities of yeast strains and human fibroblasts were

*To whom correspondence should be addressed.
†*Abbreviations:* ADH, alcohol dehydrogenase; CCD, charge-coupled device; CHO, Chinese hamster ovary; CW, continuous wave; NA, numerical aperture; NADH, nicotinamide adenine dinucleotide; NADPH, nicotinamide adenine dinucleotide phosphate; NIR, near infrared, PBS, phosphate-buffered saline; UVA, ultraviolet radiation of 320–400 nm.

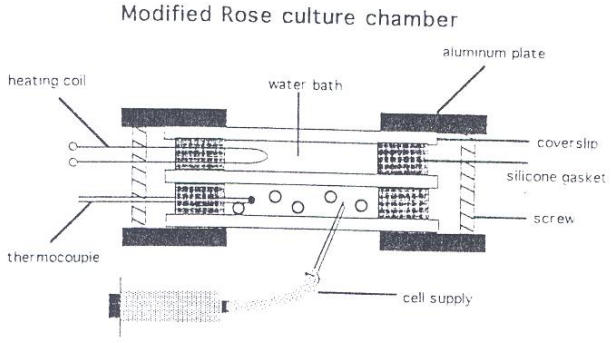

Figure 1. Schematic diagram of modified Rose culture cell chamber used for controlling temperature and maintaining sterile environment.

correlated with the function of the mitochondrial respiratory chain.[12,13] Autofluorescence changes have also been used as a method to detect cellular and tissue damage.[14]

In this paper we demonstrate that microspectrofluorometry can be used to probe the physiological status (relative redox state) of optically trapped cells. Our goal was to develop a real-time optical method for probing the effects of two trapping wavelengths: 1064 nm and 760 nm. Our results show that 1064 nm microbeams can be applied for an extended period without inducing autofluorescence changes characteristic of alterations in the cellular redox state. In contrast, 760 nm microbeams appear to produce an autofluorescence increase similar to UVA (320–400 nm) exposure. We propose that 760 nm effects are a consequence of a two-photon absorption mechanism, which alters the cellular redox balance and, in a manner similar to UVA exposure, places the cell in a state of oxidative stress.

MATERIALS AND METHODS

Chemicals. The β-NADH and β-NADPH (disodium salt) were obtained from Sigma (St. Louis, MO); 1 ng/mL β-NADH is equivalent to 1.28 m*M* based on a molecular weight of 781, which includes 4 moles water. The reduced coenzymes were dissolved in phosphate-buffered saline (PBS), pH 7.4, and promptly used. Alcohol dehydrogenase (ADH, Sigma) was used in a final concentration of 10 μ*M*.

Cell and cell culture. Chinese hamster (*Cricetulus griseus*) ovary cells (CHO, ATCC no. 61) were maintained in GIBCO's minimum essential medium (10% fetal bovine serum). Cells were subcultured in T-25 tissue culture flasks twice a week using 0.25% trypsin for digestion. For experimentation, suspended cells were diluted in PBS (pH 7.4) and injected into a modified Rose culture chamber.[15] Experiments were carried out at 25°C and culture chamber temperature was monitored continuously using a thermocouple probe.

Sample holder. The modified Rose culture chamber consisted of two separate chambers, as shown in Fig. 1. The lower one contained the cells, two injection needles connected with polyethylene tubing for cell loading and a copper–constantin thermocouple (Omega Engineering, Stamford, CT) for temperature measurements. Thermovoltage was measured by means of a Hewlett-Packard 348 B voltmeter. The upper chamber contained a heated water reservoir controlled by a heating coil driven by an electrical current (Hewlett-Packard 6236 B power supply). The cell injection needle was positioned such that video-controlled cell entrance into the medium was possible.

Experimental set-up. The scheme of the modified microscope for laser-induced optical trapping and microspectrofluorometry is shown in Fig. 2. The trapping beam was provided by a continuous-wave (CW) Nd:YAG laser (Quantronix model 114, Smithtown, NY) operating at 1064 nm in the TEM_{00} mode. The beam was coupled to an inverted 760 mm Nikon microscope and focused onto the specimen plane by a Leitz 100× objective (NA = 1.2, water immersion). An oil immersion objective was not used, because usual immersion oil (Zeiss, 518C) was found to induce a background emission in the blue spectral region. The actual *in situ* NIR power reaching the sample was determined by measuring the laser power in air before entering the objective and applying a correction factor that, for a given objective, accounts for lens transmission as well as water and glass refractive indices encountered during cell irradiation.[16] For example, 100 mW measured at 1.06 μm corresponds to an *in situ* power of approximately 53 mW. All sample exposure values are reported in terms of these corrected power levels. Previously measured spot sizes using the knife-edge technique ranged between 0.8 and 0.9 μm for a similar trapping system.[16] We therefore assumed diffraction-limited spots in this work could be approximated by $d = \lambda/NA$, where λ and NA are, respectively the laser wavelength and objective numerical aperture.

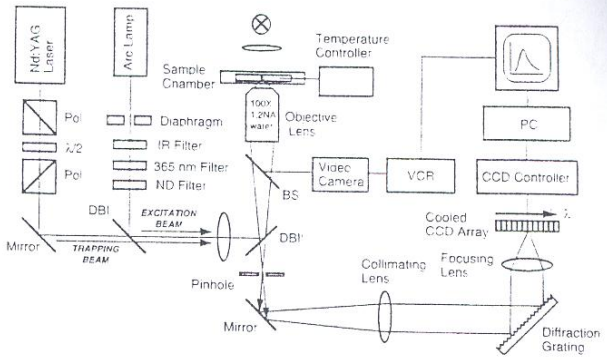

Figure 2. Experimental set-up for fluorescence spectroscopy on optically trapped CHO cells. The beamsplitter (BS) reflects visible and NIR light either to an eyepiece equipped with an NIR/IR blocking filter or to a videocamera for monitoring cell trapping, cell size and position of the trapped cell within the fluorescence detection area. The dichroic mirror (DB II) inside the microscope reflects both the NIR trapping radiation and the UV excitation and transmits fluorescence radiation at wavelengths >400 nm.

A 200 W high-pressure mercury arc lamp (model 66006, Oriel Inc., Stamford, CT) equipped with an IR-blocking filter and a 365 ± 25 nm bandpass interference filter was used as the fluorescence excitation source. The UVA was launched into the microscope colinearly with NIR radiation using a series of dichroic mirrors. Irradiation time was controlled by a computer-driven electronic shutter (Uniblitz model T132, Vincent Associates, Rochester, NY). The corrected *in situ* UVA power was determined to be 10 μW. A uniform spot diameter of 35 μm was estimated from the processed fluorescence image of a rhodamine solution injected into the Rose culture chamber. Thus, a UVA radiation intensity of about 1 W/cm² was applied.

Fluorescence was collected by the same objective and directed to the entrance slit of a polychromator (300 g/mm grating). An adjustable pinhole at the image plane of the objective allowed fluorescence detection of small sample areas (typically 15 μm in diameter). Spectra were recorded (370–615 nm) with a cooled charge-coupled device (CCD) camera (Princeton Instruments, model TE576/ST135, Trenton, NJ) and analyzed by a personal computer. Each spectrum was acquired in 1 s and corrected spectra were determined from correction factors obtained with an NBS-calibrated light source (model 5506C, Optronic Labs, Orlando, FL).

For studies with a 760 nm trapping beam, another experimental set-up with a tunable, CW Ti:sapphire laser (899-01 ring laser equipped with 3 plate birefringent filter, Coherent, Palo Alto, CA) and a modified confocal laser scanning microscope (Zeiss Axiovert 135 LSM, Germany) equipped with the cooled CCD camera was used. Assuming a diffraction-limited spot size, an IR intensity of 50 MW/cm² (160 mW) was estimated. In this mode, the CCD was used to record the spatially integrated cellular fluorescence signal over the wavelength range of 400–600 nm by a combination of 400 nm

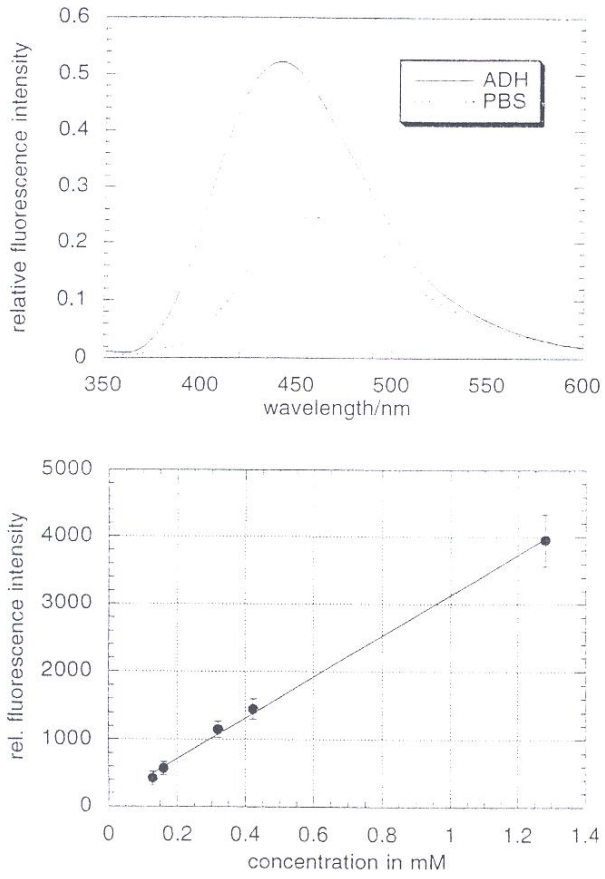

Figure 3. (a) Fluorescence emission spectra of free 0.1 m*M* NADH and protein-bound NADH (NADH–ADH mixture, [ADH] = 10 μ*M*) in PBS. (b) Relative fluorescence intensity at 457 nm *vs* concentration of NADH in PBS.

long-pass and 600 nm short-pass filters. Fluorescence excitation was, as before, provided by the 365 nm line of a 100 W mercury-arc lamp isolated with a narrowband interference (G365, Zeiss) and directed onto the sample with an FT395 (Zeiss) dichroic filter.

RESULTS

Fluorescence calibration

In order to establish the analytical performance of our microspectrofluorometric instrument, fluorescence studies were performed on coenzyme solutions injected into Rose chambers. The detector aperture was adjusted to restrict fluorescence signals to a 10 μm diameter sample spot (*i.e.* cellular dimensions). Figure 3a shows corrected NADH emission spectra. A main peak at 457 nm is visible for free NADH solutions. In contrast, mixtures of NADH and the enzyme ADH exhibit a blue-shifted maximum at 442 nm. The fluorescence quantum yield of the NADH–ADH mixture is a factor of two higher than protein-free solution. The dependence of the peak fluorescence intensity on free NADH concentration is depicted in Fig. 3b. These results demonstrate that reasonable linearity, sensitivity and spectral resolution can be achieved for small volume measurements of NADH at concentrations typically encountered in cells. Application of UV excitation (300 J/cm^2) to a 0.13 m*M* solution resulted in a fluorescence decrease of only 5%, indicating that no significant photobleaching of free NADH occurs under these conditions.

Determination of minimum trapping power

Cells were trapped at 1064 nm with an *in situ* power of 100 mW and raised to a height of about 10 μm above the glass bottom to avoid cell attachment. In order to assess the minimum laser power required for trapping, the light intensity was gradually diminished by iteratively rotating the polarizer and translating the sample chamber along one horizontal axis. Minimum trapping power was determined when the cell could no longer be held. An average value of 28.1 ± 4.4 mW was measured for 10 cells (mean diameter 11.0 ± 1.9 μm). Because we typically use trapping powers that exceed minimum values, *e.g.* to confine motile cells, we selected 100, 230 and 460 mW for subsequent autofluorescence monitoring studies.

Autofluorescence studies

The 365 nm excited autofluorescence of 20 trapped cells for each of the standard power levels (100 mW, 230 mW and 460 mW) was measured immediately (about 5 s) after the start of 1064 nm trapping. However, no dependence of fluorescence intensity and spectral characteristics on trapping power was found. The peak autofluorescence intensity of single, optically trapped CHO cells corresponded to that of 0.1 m*M* free NADH in aqueous solution (see Fig. 3b). A mean fluorescence standard deviation of about 30% was observed, indicating a high variability in the concentration of endogenous fluorophores, probably due to size and cell cycle differences. All cells showed a fluorescence maximum at around 455 nm.

In order to acquire information on autofluorescence changes from cells trapped for a more extended period, 10 cells were chosen to be trapped for a period of 1 h (trap power = 230 mW, λ = 1064 nm, light intensity: 37 MW/cm^2). Cell fluorescence was recorded every 10 min. Two samples showed a strong fluorescence increase. However, this was caused by the sudden incorporation of an additional cell in the same trap. Two other cells exhibited a significant fluorescence decrease concomitant with membrane damage and cell lysis. Figure 4 summarizes the time-dependent fluorescence behavior for the eight single-cell recordings over a total radiant exposure of 134 GJ/cm^2.

Next, we studied the influence of 760 nm microbeams on cellular autofluorescence. Ten cells were trapped with a constant light intensity of about 50 MW/cm^2 at 760 nm and autofluorescence was recorded in 5 min time intervals. Interestingly, nine cells exhibited a significant fluorescence increase with trapping time. As demonstrated in Fig. 4, up to a factor of two increase in fluorescence intensity was observed at 22 min (66 GJ/cm^2). One cell showed no significant changes.

Because the 1064 nm traps did not appear to influence cellular autofluorescence, we employed this wavelength as a micromanipulation tool to study the impact of UVA exposure on single CHO cells. Ten cells were trapped at 1064 nm (460 mW) for 10 min and then, in the optical trap, continuously exposed to the mercury lamp. Fluorescence spectra

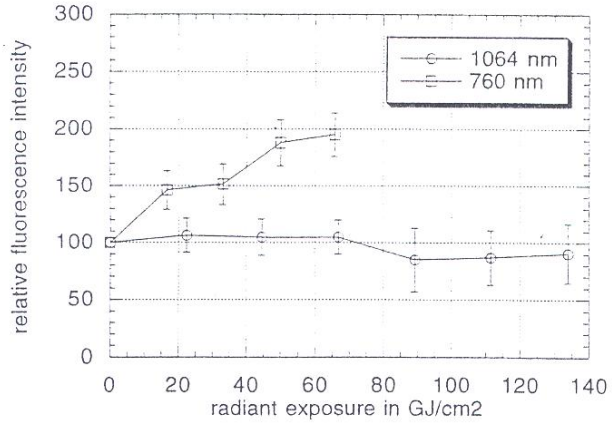

Figure 4. Relative autofluorescence intensity *vs* radiant exposure for cells trapped with 1064 nm and 760 nm microbeams.

ere acquired from each cell over a period of up to 24 min while in the trap. Spectra were recorded in blocks of 120 s (1 spectrum per second; 0.2 s read time) corresponding to an applied UVA radiant exposure of 120 J/cm^2 every 2 min. The dark period between consecutive series of 100 spectra was 5 s.

Figure 5a shows the fluorescence intensity *vs* wavelength (400–500 nm) and radiant exposure for a single trapped cell. These data clearly demonstrate that UVA has a dramatic effect on cellular autofluorescence intensity and spectra. Closer examination of the 460 nm fluorescence kinetics curve (Fig. 5b) reveals that during the first exposure phase (up to 120 J/cm^2), fluorescence intensity appears to decrease. The UVA radiant exposure at which the fluorescence intensity drops to a minimum value occurs at about 120 J/cm^2 for this particular cell. Interestingly, this minimum autofluorescence intensity of one-half to one-third of the initial value (I_0) is followed by a significant fluorescence increase of two to three times I_0 during further UVA exposure. Figure 5b also shows that fluorescence levels from the last spectrum of each series are lower than the intensities seen in the first spectrum of the following series. This jump is suggestive of dark reactions because cells were not exposed to UVA for a period of 5 s while data were assigned a file name and written to the hard disk. In the third exposure phase, fluorescence reaches a value of about 2.5 times I_0 after 14 min (840 J/cm^2). When the cell was maintained in the dark for an additional 10 min, a new fluorescence maximum with a 4.5-fold higher value than I_0 was observed at the start of the final series of 100 spectra (numbers 800–900). This transient intensity increase disappeared during the final recording series to a level close to the previous maximum. The mean relative fluorescence maxima and minima for 10 cells (±standard deviations) were determined to be: I_{max}/I_0 = 1.8 ± 0.6 and I_{min}/I_0 = 0.3 ± 0.1. Corresponding mean times (t_{min} and t_{max}) required to achieve these levels were 179 ± 86 s and 880 ± 162 s, respectively, and the mean relative intensity following the dark period (I_{dark}/I_0) was 4.3 ± 0.9.

In addition to modifications in fluorescence intensity, a red shift of the fluorescence maximum and an increased ratio of 460 nm (free NADH) to 440 nm (protein-bound peak) were observed for the Fig. 5 cell. Protein-bound NADH has a two-

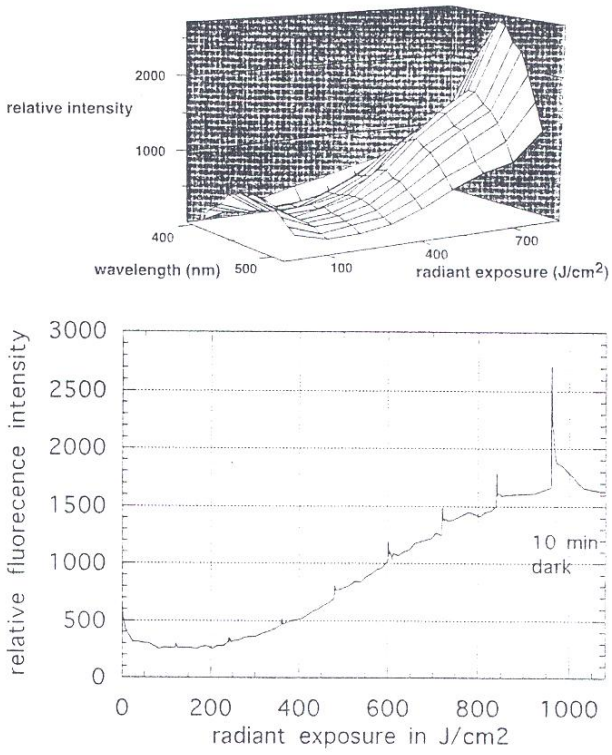

Figure 5. (a) Relative autofluorescence intensity *vs* wavelength and UVA radiant exposure for a single cell. A total of 900 spectra were acquired. Plots contain data from nine spectra, numbers 1, 101, 201, 301, 401, 501, 601, 701 and 801. Spectrum 801 was obtained after a dark phase of 10 min. (b) Relative autofluorescence intensity at 460 nm *vs* UVA radiant exposure for a single cell (same cell as in Fig. 5a).

fold higher quantum yield than the free form. An increase in the 460/440 fluorescence intensity ratio can be attributed either to a decrease in the protein-bound component or an increase in free NADH. Because an overall fluorescence increase is observed during UVA irradiation, these data, summarized in Fig. 6 for a single cell, suggest rather complex NADH dynamics.

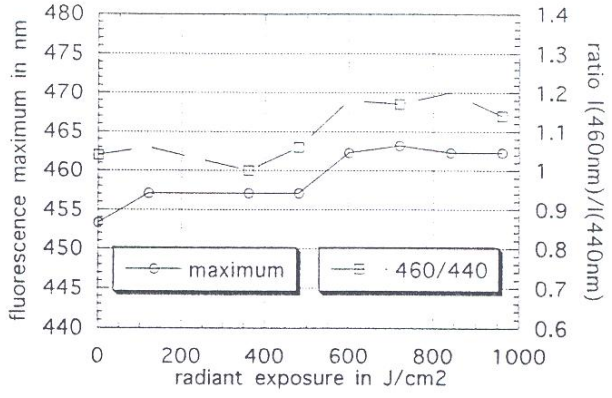

Figure 6. Variation in autofluorescence emission maximum and ratio of free (I_F (460 nm)) to protein-bound (I_F (440 nm)) fluorescence components for a single cell (same cell as in Fig. 5a) during UVA exposure.

DISCUSSION

Excitation of CHO cells at 365 nm results in broad-band fluorescence emission spectra with maxima typical for the reduced coenzyme NADH. The peak autofluorescence intensity of single, optically trapped CHO cells corresponds to that of 0.1 m*M* free NADH in aqueous solution. Taking into account the fact that bound NADH exhibits up to a three-fold increase in fluorescence intensity, an intracellular NAD(P)H concentration between 30 μM and 100 μM can be estimated. This value corresponds with data from the literature.[17,18]

Although autofluorescence measurements during 1064 nm cell trapping did not produce significant signal alterations, 90% of the investigated cells experience significant autofluorescence changes during exposure to 760 nm light. Previous work has shown that 760 nm microirradiation on glass-attached cells affects mitosis.[19] Because reduced forms of hemoglobin and cytochromes exhibit small but significant absorption at 760 nm,[20] potential molecular targets for short-wavelength NIR absorption include tetrapyrrolic chromophores such as the deoxyhemoglobin "band III" (α[760] = 4.5 cm^{-1}) and the ferroheme a3 charge transfer band of cytochromes[21,22]; water absorption (~0.01 cm^{-1}) is negligible.[23] In contrast, NIR water absorption at 1064 nm is 10× greater (~0.1 cm^{-1}) and, due to the absence of other endogenous chromophores, is generally thought to be the primary absorber in this spectral region.[24]

Two-photon absorption can also occur in the case of CW laser microbeams.[25] As mentioned, light intensities of about 50 MW/cm^2 are induced in the 760 nm trap. This corresponds to a photon flux density of 10^{27} photons cm^{-2} s^{-1}. Simultaneous absorption of two photons typically requires photon flux densities of about 10^{25} photons cm^{-2} s^{-1}.[26,27] Therefore, two-photon absorption has to be considered in CW optical traps. Indeed, we have observed two-photon-excited visible fluorescence and a quadratic power dependence in optically trapped single cells.[28] As a result, 760 nm microbeams may induce biological effects that are similar to one-photon UVA effects (760 nm/2 = 380 nm). In contrast to 1064 nm (1064 nm/2 = 532 nm) light, two-photon molecular targets using short-wavelength NIR radiation are more abundant and highly absorbing in cells.

Significant changes in cellular autofluorescence also occurred during UVA exposure. Although average light intensities from the mercury-arc lamp were 10^7 less than those of the Ti:sapphire laser, the entire cell was uniformly exposed to UVA. In contrast, the NIR beam was focused to a submicron spot. As a result, the primary damage site for both one- and two-photon NIR effects would be highly localized, the latter to a particularly small region of the focused beam.[29] Consequently, substantially larger populations of molecular absorbers are accessible with arc-lamp illumination. Examples of efficient absorbers in this spectral region include: endogenous porphyrins (metal free and metalloporphyrins), pyridine coenzymes and flavin molecules.

An initial decrease in autofluorescence was detected at UVA radiant exposures of 1–120 J/cm^2. This first phase of reduction in fluorescence may be attributable to UVA-induced oxidation processes, which convert NAD(P)H into nonfluorescent NAD(P). This could occur *via* well-known type I and II photooxidation mechanisms (involving superoxide [O_2^-] and singlet oxygen [$^1O_2$], respectively) where NAD(P)H and flavins act as photosensitizers.[30,31] At longer times photogenerated oxygen species can cause oxidative stress and cell lysis by lipid peroxidation, membrane and DNA damage and enzyme inactivation. It has been reported that NADH photosensitization plays a role in UV-induced DNA strand breaks.[30,31] Lubart *et al.*[32] found inhibition of cell mitosis after 360 nm exposure in the J/cm^2 range. These effects could explain our observation that UVA radiant exposures greater than 120 J/cm^2 result in significant increases in fluorescence (up to 550% of initial levels). Possible mechanisms for this signal increase during light stress can be alterations in the cellular redox balance due to increased NADH levels, NADH efflux from defective mitochondria and coenzyme binding with cytoplasmic and nuclear proteins. Although alterations in fluorescence did not appear to correlate with immediate visible morphological changes, cells were generally unable to exclude trypan blue (a membrane-impermeant viability probe) at radiant exposures greater than 250–350 J/cm^2. This suggests that UVA-induced membrane damage and viability loss probably occurred at some point during the rise in cellular autofluorescence levels. Trypan blue incorporation was similarly observed at approximately 8–15 GJ/cm^2 of 760 nm irradiation. In contrast, cell viability, as indicated by trypan blue exclusion, did not appear to be affected for up to 140 GJ/cm^2 of 1064 nm irradiation.

Further work is necessary to correlate autofluorescence changes with additional cell damage and viability assays in order to determine whether this is a useful probe of cell physiology in optical traps. Nevertheless, these studies demonstrate that microspectrofluorometry can be combined with optical tweezers to interrogate the redox state of single cells. This can be particularly useful in the case of motile cells where single cell spectroscopic recordings cannot easily be obtained using conventional means. In addition, we have begun to apply this "pump-probe" approach to optically trapped cells that have incorporated exogenous fluorescent probes. Collectively, these techniques provide a novel means for understanding the impact of light on cell function and may lead to a more complete description of the relationship between one-photon and two-photon UVA and NIR effects.

Acknowledgements—This work has been performed with support from the National Institutes of Health (5P41RR01192-15), the Office of Naval Research (N00014910134) and the Dept. of Energy (DE-FG391ER61227). Additional funding to K.K. from Deutsche Forschungsgesellschaft (DFG) is gratefully acknowledged.

REFERENCES

1. Ashkin, A. (1970) Acceleration and trapping of particles by radiation pressure. *Phys. Rev. Lett.* **24**, 156–159.
2. Ashkin, A. J. M. Dziedzic, J. E. Bjorkholm and S. Chu (1986) Observation of a single-beam gradient force optical trap for dielectric particles. *Opt. Lett.* **11**, 288–290.
3. Ashkin, A. and J. M. Dziedzic (1987) Optical trapping and manipulation of viruses and bacteria. *Science* **235**, 1517–1520.
4. Block, S. M., D. F. Blair and H. C. Berg (1989) Compliance of bacterial flagella measured with optical tweezers. *Nature* **338**, 514–518.
5. Buican, T. N., M. J. Smith, H. A. Crissmann, G. C. Salzmann, C. C. Stewart and J. C. Martin (1987) Automated single-cell

manipulation and sorting by light trapping. *Appl. Opt.* **26**, 5311–5316.
6. Berns, M. W., W. H. Wright, B. J. Tromberg, G. A. Profeta, J. J. Andrews and R. I. Walter (1989) Use of a laser-induced optical force trap to study chromosome movement on the mitotic spindle. *Proc. Natl. Acad. Sci. USA* **86**, 4539–4543.
7. Tadir, Y., W. H. Wright, O. Vafa, T. Ord, R. H. Asch and M. W. Berns (1990) Force generated by human sperm correlated to velocity and determined using a laser generated optical trap. *Fertil. Steril.* **53**, 944–947.
8. Siegman, A. E. (1986) *Lasers*. University Science Books, Mill Valley, CA.
9. Chance, B. C. and B. Thorell (1959) Localization and kinetics of reduced pyridine nucleotides in living cells by microfluorimetry. *J. Biol. Chem.* **234**, 3044–3050.
10. Mayevski, A. (1984) Brain NADH redox state monitored *in vivo* by fiber optic surface fluorometry. *Brain Res. Rev.* **7**, 49–68.
11. Lohmann, W. (1988) *In situ* detection of melanomas by fluorescence measurements. *Naturwissenschaften* **75**, 201–202.
12. Schneckenburger, H., P. Gessler and I. Pavenstädt-Grupp (1992) Measurement of mitochondrial deficiencies in living cells by microspectrofluorometry. *J. Histochem. Cytochem.* **40**, 1573–1578.
13. Schneckenburger, H. and K. König (1992) Fluorescence decay kinetics and imaging of NAD(P)H and flavins as metabolic indicators. *Opt. Eng.* **31**, 1447–1451.
14. König, K. and H. Schneckenburger (1994) Laser-induced autofluorescence for medical diagnosis. *J. Fluoresc.* **4**, 17–40.
15. Rose, G. (1954) A separable and multipurpose tissue culture chamber. *Tex. Rep. Biol. Med.* **12**, 1074–1083.
16. Wright, W. H., G. J. Sonek and M. W. Berns (1994) Parametric study of the forces on microspheres held by optical tweezers. *Appl. Opt.* **33**, 1735–1748.
17. Liang, B. and H. R. Petty (1992) Imaging neutrophil activation: analysis of the translocation and utilization of NAD(P)H-associated autofluorescence during antibody-dependent target oxidation. *J. Cell. Physiol.* **152**, 145–156.
18. Guezennec, C. Y., F. Lienhard, F. Louisy, G. Renault, M. H. Tusseau and P. Portero (1991) *In situ* NADH laser fluorimetry during muscle contraction in humans. *Eur. J. Appl. Physiol.* **63**, 36–42.
19. Vorobjev, I. A., H. Liang, W. H. Wright and M. W. Berns (1993) Optical trapping of chromosome manipulation: a wavelength dependence of induced chromosome bridges. *Biophys. J.* **64**, 533–538.
20. Wray, S., M. Cope, D. T. Delpy, J. S. Wyatt and E. O. R. Reynolds (1988) Characterization of the near-infrared absorption spectra of cytochrome aa_3 and hemoglobin for the non-invasive monitoring of cerebral oxygenation. *Biochim. Biophys. Acta* **933**, 184–192.
21. Ingledew, W. J., M. Bacon and P. R. Rich (1992) Characterization of a near-infrared absorption band of the *Escherichia coli* quinol oxidase, cytochrome o, which is attributable to the high-spin ferrous haem of the binuclear site. *FEBS Lett.* **305**, 167–170.
22. Rich, P. R., A. J. Moody and W. J. Ingledew (1992) Detection of a near infra-red absorption band of ferrohaem a3 in cytochrome c oxidase. *FEBS Lett.* **305**, 171–173.
23. Hale, G. M., and M. R. Querry (1973) Optical constants of water in the 200 nm to 200 μm wavelength region. *Appl. Opt.* **12**, 555–563.
24. Liu, Y., D. K. Cheng, G. J. Sonek, M. W. Berns, C. F. Chapman and B. J. Tromberg (1995) Evidence for localized cell heating induced by infrared optical tweezers. *Biophys. J.* **68**, 2137–2144.
25. Hänninen, P. E., E. Soini and S. W. Hell (1994) Continuous wave excitation two-photon fluorescence microscopy. *J. Microsc.* **176**, 222–225.
26. Hermann, J. P. and J. Ducuing (1972) Absolute measurements of two-photon cross sections. *Phys. Rev.* **A5**, 2557–2568.
27. Kennedy, S. M., and F. E. Lytle (1986) P-bis(*o*-methylstyryl)benzene as a power squared tensor for two-photon absorption measurements between 537 and 694 nm. *Anal. Chem.* **58**, 2643–2647.
28. König, K., Y. Liu, T. Krasieva, P. Patrizio, Y. Tadir, G. J. Sonek, M. W. Berns and B. J. Tromberg (1995) Fluorescence imaging and spectroscopy of motile sperm cells and CHO cells in an optical trap ("laser tweezers"). *J. Soc. Photo-Opt. Instrum.* **2391**, 238–249.
29. Denk, W., J. H. Strickler and W. W. Webb (1990) Two-photon laser scanning fluorescence microscope. *Science* **248**, 73–76.
30. Burchuladze, T. G., E. G. Sideris and G. I. Fraikin (1990) Sensitized NADH formation of single-stranded breaks in plasmid DNA upon the action of near UV radiation. *Biofizika* **35**, 722–725.
31. Cunningham, M. L., J. S. Johnson, S. M. Giovanazzi and M. J. Peak (1985) Photosensitized production of superoxide anion by monochromatic (290–405 nm) ultraviolet irradiation of NADH and NADPH coenzymes. *Photochem. Photobiol.* **42**, 125–128.
32. Lubart, R., Y. Wollman, H. Friedmann, S. Rochkind and I. Laulicht (1992) Effects of visible and near-infrared lasers on cell cultures. *J. Photochem. Photobiol. B* **12**, 305–310.